doi: 10.4149/gpb_2020041

circCUX1 promotes neuroblastoma progression and glycolysis by regulating the miR-338-3p/PHF20 axis

Yan Wang[1], Qin Niu[2], Jie Dai[1], Haitang Shi[1] and Jinzhi Zhang[1]

[1] *Department of Neonatology, The First People's Hospital of Lianyungang, Lianyungang, Jiangsu, China*
[2] *Department of Oncology, The First People's Hospital of Lianyungang, Lianyungang, Jiangsu, China*

Abstract. Neuroblastoma (NB) is an extracranial solid malignancy in childhood. More and more studies have demonstrated that circRNAs are essential regulators of various tumors. This study conducted to explore the role and mechanism of circular RNA CUT-like homeobox 1 (circCUX1) in NB. The levels of circCUX1, miR-338-3p and plant homeodomain finger protein 20 (PHF20) were detected by qRT-PCR or Western blot. Cell proliferation and apoptosis were evaluated by colony formation assay, flow cytometry and Western blot analysis. Cell migration and invasion were examined *via* transwell assay. Glycolysis was expressed by measuring the extracellular acidification rate (ECAR). The interaction among circCUX1, miR-338-3p and PHF20 were validated by dual-luciferase reporter assay and RNA Immunoprecipitation assay. Besides, xenograft experiment was performed to assess tumor growth *in vivo*. circCUX1 and PHF20 were up-regulated, while miR-338-3p was down-regulated in NB tissues and cells. Knockdown of circCUX1 suppressed the progression and glycolysis of NB cells. circCUX1 triggered NB progression and glycolysis by regulating miR-338-3p. Additionally, down-regulation of miR-338-3p promoted NB progression and glycolysis *via* targeting PHF20. Moreover, circCUX1 sponged miR-338-3p to regulate PHF20 expression. Furthermore, circCUX1 silencing hindered tumor growth *in vivo*. circCUX1 depletion suppressed tumor progression and glycolysis in NB by regulating miR-338-3p/PHF20 axis, suggesting a potential biomarker for NB treatment.

Key words: Neuroblastoma – circCUX1 – miR-338-3p – PHF20 – Glycolysis

Abbreviations: circCUX1, circular RNA CUT-like homeobox 1; ECAR, extracellular acidification rate; NB, neuroblastoma; PHF20, plant homeodomain finger protein 20.

Introduction

Neuroblastoma (NB) is the most frequent extracranial solid tumor in children and the main cause of high mortality in pediatric cancer, accounting for approximately 15% of childhood cancer-related mortality (Matthay 1995; Maris et al. 2007). Also, NB is a heterogeneous disease characterized by natural regression and a high rate of metastasis (Brodeur and Bagatell 2014). Recently, tumor biology has optimized the classification of NB, and some new targeted therapies have made significant progress, resulting in improved clinical efficacy of highly aggressive NB (Louis and Shohet 2015). Nevertheless, the potential mechanism of this tumor is still not completely understood, and we need to further explore the molecular mechanism in NB development to provide new treatment options.

Circular RNAs (circRNAs) are formed by cyclization of exons or introns at the 3' and 5' ends (Kristensen et al. 2019). Accumulating evidence has highlighted that circRNAs exert a regulatory effect on various biological and pathological processes *via* serving as microRNA (miRNA) sponges (Cui et al. 2018). For example, circFAM114A2 sponged miRNA-762 to block the malignancy of bladder cancer by activating NP63 (Liu et al. 2020). In addition,

Correspondence to: Qin Niu, Department of Oncology, The First People's Hospital of Lianyungang, No. 6, Zhenhua East Road, Haizhou District, Lianyungang City, Jiangsu Province, 222000, China
E-mail: leleliuhai@163.com

circFOXM1 silencing suppressed the progression of papillary thyroid carcinoma *via* modulating miRNA-1179/HMGB1 pathway (Ye et al. 2020). Also, circ-ENO1 facilitated tumorigenesis and glycolysis in lung adenocarcinoma *via* sponging miRNA-22-3p to elevate ENO1 expression (Zhou et al. 2019). Furthermore, Li et al. (2019) unveiled that hsa_circ_0132813 derived from CUT-like homeobox 1 (CUX1) was significantly up-regulated in NB, and circCUX1 silencing restrained glycolysis and growth of NB cells. Nevertheless, the potential mechanism of circCUX1 has not been clarified.

Moreover, mounting evidence has manifested that miRNAs play a critical role in the occurrence and development of NB by binding to mRNA 3'UTR to regulate gene expression (Fabian et al. 2010; Farazi et al. 2011). For instance, miR-149 suppressed cell growth and doxorubicin sensitivity in NB *via* interacting with CDC42 and BCL2 (Mao et al. 2019). Additionally, up-regulation of miR-181a/b triggered cell proliferation and metastasis in NB by down-regulating ABI1 (Liu et al. 2018). Moreover, miR-221 overexpression expedited MYCN-induced NB *via* binding to nemo-like kinase (He et al. 2017). Bioinformatics analysis indicated that circCUX1 might bind to miR-338-3p. Hence, we speculated that circCUX1 modulated NB development by mediating miR-338-3p.

Plant homeodomain finger protein 20 (PHF20) plays an essential role in Akt signaling pathway by acting as a substrate of Akt (Park et al. 2012). PHF20 mediates PKB phosphorylation *via* functioning as a PKB substrate, which participates in tumorigenesis by affecting p53-related signaling (Li et al. 2013). In NB, PHF20 is a tumor-promoting factor (Long et al. 2018). In addition, to maintain tumor cell growth and metastasis, the process of metabolizing glucose to lactic acid under aerobic conditions is called aerobic glycolysis or Warburg effect (Vander Heiden et al. 2009).

In this research, we illuminated the function of circCUX1 in NB development. Furthermore, we investigated the correlation between circCUX1 and miR-338-3p/PHF20 axis. Our findings revealed that circCUX1 might be a therapeutic target for NB.

Materials and Methods

Clinical specimens

NB tissues ($n = 35$) and matched normal tissues ($n = 35$) were acquired from The First People's Hospital of Lianyungang. The diagnosis of NB patients was confirmed by pathologists. All participants were informed of the experimental purpose and signed written informed consent. This research was ratified by the Ethics Committee of The First People's Hospital of Lianyungang.

Cell culture

Human umbilical vein endothelial cell line HUVEC and NB cell lines (IMR32 and SHEP) were commercially acquired from Tongpai Biotech (Shanghai, China) and incubated in RPMI-1640 medium (Youkang Biotech, Beijing, China) containing 10% fetal bovine serum (FBS; Youkang Biotech) in 5% CO_2 at 37°C.

Cell transfection

circCUX1 small interfering RNA (siRNA) (si-circCUX1), PHF20 siRNA (si-PHF20), the siRNA control (si-NC), miR-338-3p mimic, the mimic control (miR-NC mimic), circCUX1 overexpression vector (oe-circCUX1), the empty overexpression vector (Vector), miR-338-3p inhibitor and negative control (miR-NC inhibitor) were bought from GenePharma (Shanghai, China). Cell transfection was carried out using Lipofectamine 3000 (Invitrogen, Carlsbad, CA, USA).

Quantitative Real-time PCR (qRT-PCR)

Trizol reagent (Invitrogen) was utilized for RNA extraction. Then, the complementary DNA generated from 500 ng RNA using the specific reverse transcription kit (Vazyme, Nanjing, China) was subjected to qRT-PCR using TB Green Fast qPCR Mix (Takara, Dalian, China). The primer sequences included: circCUX1-F: 5'-AGTGAGCAGTCCAGAAAGCG-3', circCUX1-R: 5'-AAGAAACGGGTTGTTTGCCG-3'; CUX1-F: 5'-GAAGAACCAAGCCGAAACCAT-3', CUX1-R: 5'-AGGCTCTGAACCTTATGCTCA-3'; miR-338-3p-F: 5'-TGCGGTCCAGCATCAGTGAT-3', miR-338-3p-R: 5'-CCAGTGCAGGGTCCGAGGT-3'; PHF20-F: 5'-GAATCAGCTTTGAAGTGGGAGC-3', PHF20-R: 5'-GTTCCAACGCTTGAAATGGATG-3';GAPDH-F:5'-GGGAAACTGTGGCGTGAT-3', GAPDH-R: 5'-GAGTGGGTGTCGCTGTTGA-3'; U6-F: 5'-CTCGCTTCGGCAGCACA-3', U6-R: 5'-AACGCTTCACGAATTTGCGT-3'. GAPDH and U6 were regarded as internal references.

Actinomycin D and RNase R treatment

To suppress transcription, HUVEC cells were treated with 2 mg/ml Actinomycin D (Sigma, St. Louis, MO, USA), and the expression levels of circCUX1 and CUX1 were examined using qRT-PCR at different time. For RNase R treatment, 2 μg RNA was incubated with or without RNase R (3 U/μg) (Epicentre, Madison, WI, USA) for 30 min at 37°C.

Colony formation assay

IMR32 and SHEP cells were maintained in six-well plates and continuously incubated for 14 days at 37°C in a medium

carrying 10% FBS. After fixing with methanol and staining with 0.5% crystal violet, the number of colonies was imaged and counted.

Cell apoptosis assay

IMR32 and SHEP cells were seeded into six-well plates and digested with trypsin. After washing with PBS for three times, AnnexinV-FITC and propidium iodide (PI) were added and reacted with the cells for 15 min. Next, the apoptotic rate was examined using a flow cytometer (Beckman Coulter, Miami, FL, USA).

Western blot assay

After extracting the protein with RIPA buffer (Solarbio, Beijing, China), the protein samples were separated using polyacrylamide gel electrophoresis and transferred onto polyvinylidene fluoride membranes (Sigma). After blocking with 5% non-fat milk for 2 h, the membranes interacted with primary antibodies against B cell lymphoma 2 (Bcl-2, 1:1500; ab196495, Abcam, Cambridge, UK), Bcl-2 associated X protein (Bax, 1:1000; ab53154, Abcam), PHF20 (1:1000; ab118190, Abcam) or GAPDH (1:2000; ab9485, Abcam) overnight at 4°C. Then, the membranes were probed with secondary antibody (1:20000; ab205718, Abcam). Next, the protein bands were visualized by exposing the membranes to the ECL reagent (Qiagen, Frankfurt, Germany). Western blot assay was repeated three times independently.

Transwell assay

For cell migration experiment, the treated cells were plated into the upper chamber. Meanwhile, the fresh medium containing 10% FBS was injected into the lower chamber. After staining with 0.5% crystal violet (Solarbio), the cells were photographed and counted using a microscope at magnification of 100× in three randomly selected fields. In addition, cell invasion experiment performed the same steps as cell migration experiment except for the application of Matrigel (Corning, Corning, NY, USA) in the upper chamber.

Detection of extracellular acidification rate (ECAR)

Briefly, cells (2×10^4) were seeded into a Seahorse XF 96 cell culture microplate (Seahorse Bioscience, North Billerica, MA, USA). After baseline measurements, glucose, oligomycin and 2-deoxyglucose (2-DG) were sequentially added to each well at the indicated time points. The Seahorse XF-96 Wave software was used to analyze the data. ECAR was expressed in mpH/min. All values were normalized to protein concentration.

Dual-luciferase reporter assay

The wild-type luciferase reporter plasmids (WT-circCUX1 or WT-PHF20) were formed by cloning circCUX1 or PHF20 3'UTR containing the miR-338-3p binding sequence into the pmirGLO vector (Zhen Shanghai and Shanghai Industrial Co., Ltd., Shanghai, China). The mutant luciferase reporter vectors (MUT-circCUX1 or MUT-PHF20) were generated by mutating the base at the binding site. Next, the corresponding luciferase reporter vectors were introduced into IMR32 and SHEP cells together with miR-338-3p mimic or miR-NC mimic. The luciferase activity was examined using a Dual-Lucy Assay Kit (Solarbio).

RNA immunoprecipitation (RIP) assay

IMR32 and SHEP cells were introduced with miR-338-3p mimic or miR-NC mimic. Briefly, the treated cells were lysed using RIP lysis buffer and incubated with magnetic beads conjugated with Ago2 antibody. IgG was regarded as a negative reference. The levels of circCUX1 and PHF20 in co-precipitated RNAs were examined using qRT-PCR.

Xenograft assay

The xenograft experiment was ratified by the Animal Welfare Committee of The First People's Hospital of Lianyungang. SHEP cells were transfected with lentivirus containing circCUX1 short hairpin RNA (sh-circCUX1) or negative control (sh-NC) purchased from GenePharma. Subsequently, stably transfected SHEP cells (5×10^6) were subcutaneously injected into the right abdomen of five weeks old BALB/c nude mice. Additionally, tumor volume was measured once a week. Four weeks later, the xenografts were excised and weighed.

Statistical analysis

All data were analyzed according to Graphpad Prism 7.0 software (GraphPad, San Diego, CA, USA) and displayed as mean ± standard deviation. Differences were assessed using Student's *t*-test, one-way analysis of variance (ANOVA) or two-way ANOVA. $p < 0.05$ was considered statistically significant. All experiments were performed three times independently.

Results

CircCUX1 is increased in NB tissues and cells

First, we examined the differential expression of circCUX1 in NB tissues and normal tissues. As exhibited in Figure 1A, circCUX1 expression in NB tissues was markedly

higher than that in normal tissues. Simultaneously, the expression of circCUX1 in IMR32 and SHEP cells was significantly increased compared with HUVEC cells (Fig. 1B). To detect the stability of circCUX1, HUVEC cells were treated with Actinomycin D. The results illustrated that the half-life of circCUX1 was remarkably higher than that of CUX1 mRNA (Fig. 1C). In addition, RNase R digestion assay revealed that circCUX1 was more resistant to RNase R than the linear isoform CUX1 mRNA (Fig. 1D). These data suggested that circCUX1 was highly expressed and stable in NB.

circCUX1 knockdown suppresses the progression and glycolysis of NB cells

To elucidate the effect of circCUX1 on NB development, we performed a series of loss-of-function experiments. First, si-NC or si-circCUX1 was introduced into IMR32 and SHEP cells, and the knockdown efficiency of circCUX1 was determined by qRT-PCR (Fig. 2A). Colony formation assay illustrated that transfection with si-circCUX1 inhibited NB cell proliferation relative to the si-NC group (Fig. 2B). Furthermore, silencing of circCUX1 remarkably increased the apoptosis rate of IMR32 and SHEP cells (Fig. 2C). Meanwhile, inhibition of circCUX1 caused a significant decrease in Bcl-2 level and a marked increase in Bax level (Fig. 2D). Transwell assay revealed that circCUX1 knockdown suppressed the migration and invasion of IMR32 and SHEP cells (Fig. 2E,F). Moreover, glycolysis can be reflected by detecting the rate of extracellular acidification. The results exhibited that silencing of circCUX1 strikingly reduced the ECAR compared to the control group (Fig. 2G,H). Collectively, these data indicated that depletion of circCUX1 inhibited the progression and glycolysis of NB cells.

circCUX1 directly interacts with miR-338-3p

Circular RNA Interactome online database predicted that circCUX1 had putative binding sites with miR-338-3p (Fig. 3A). To clarify whether circCUX1 bound to miR-338-3p, we performed dual-luciferase reporter assay. The results showed that miR-338-3p mimic strikingly reduced the luciferase activity of WT-circCUX1 reporter, but did not affect MUT-circCUX1 (Fig. 3B). RIP assay confirmed that circCUX1 was significantly enriched in NB cells introduced with miR-338-3p mimic (Fig. 3C). Then, the overexpression efficiency of circCUX1 was validated by qRT-PCR (Fig. 3D). Moreover, miR-338-3p expression in the si-circCUX1 group was remarkably elevated compared to the si-NC group, while miR-338-3p expression in the oe-circCUX1 group was markedly decreased relative to the Vector group (Fig. 3E). Also, miR-338-3p expression was significantly down-regulated in NB tissues, IMR32 and SHEP cells (Fig. 3F,G). Furthermore, Spearman's correlation analysis displayed that circCUX1 and miR-338-3p were negatively correlated in NB tissues (Fig. 3H). These data unveiled that circCUX1 negatively targeted miR-338-3p.

Inhibition of miR-338-3p alleviates the effect of circCUX1 knockdown on NB cells

Further, to investigate whether circCUX1 regulated NB progression by targeting miR-338-3p, IMR32 and SHEP cells were transfected with miR-NC inhibitor, miR-338-3p inhibitor, si-circCUX1+miR-NC inhibitor or si-circCUX1+miR-338-3p inhibitor. First, the inhibition efficiency of miR-338-3p was determined using qRT-PCR (Fig. 4A). Colony formation assay and flow cytometry demonstrated that miR-338-3p down-regulation induced cell proliferation and repressed apoptosis, while co-transfection

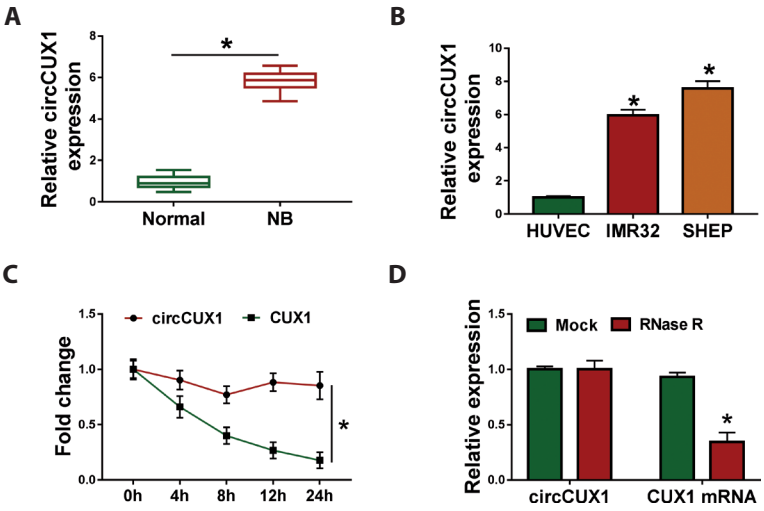

Figure 1. CircCUX1 is increased in neuroblastoma (NB) tissues and cells. **A, B.** The expression of circCUX1 was detected by qRT-PCR in NB tissues (n = 35), normal tissues (n = 35) and HUVEC, IMR32 and SHEP cells. **C, D.** After Actinomycin D stimulation or RNase R treatment, the levels of circCUX1 and CUX1 mRNA were measured by qRT-PCR. * $p < 0.05$.

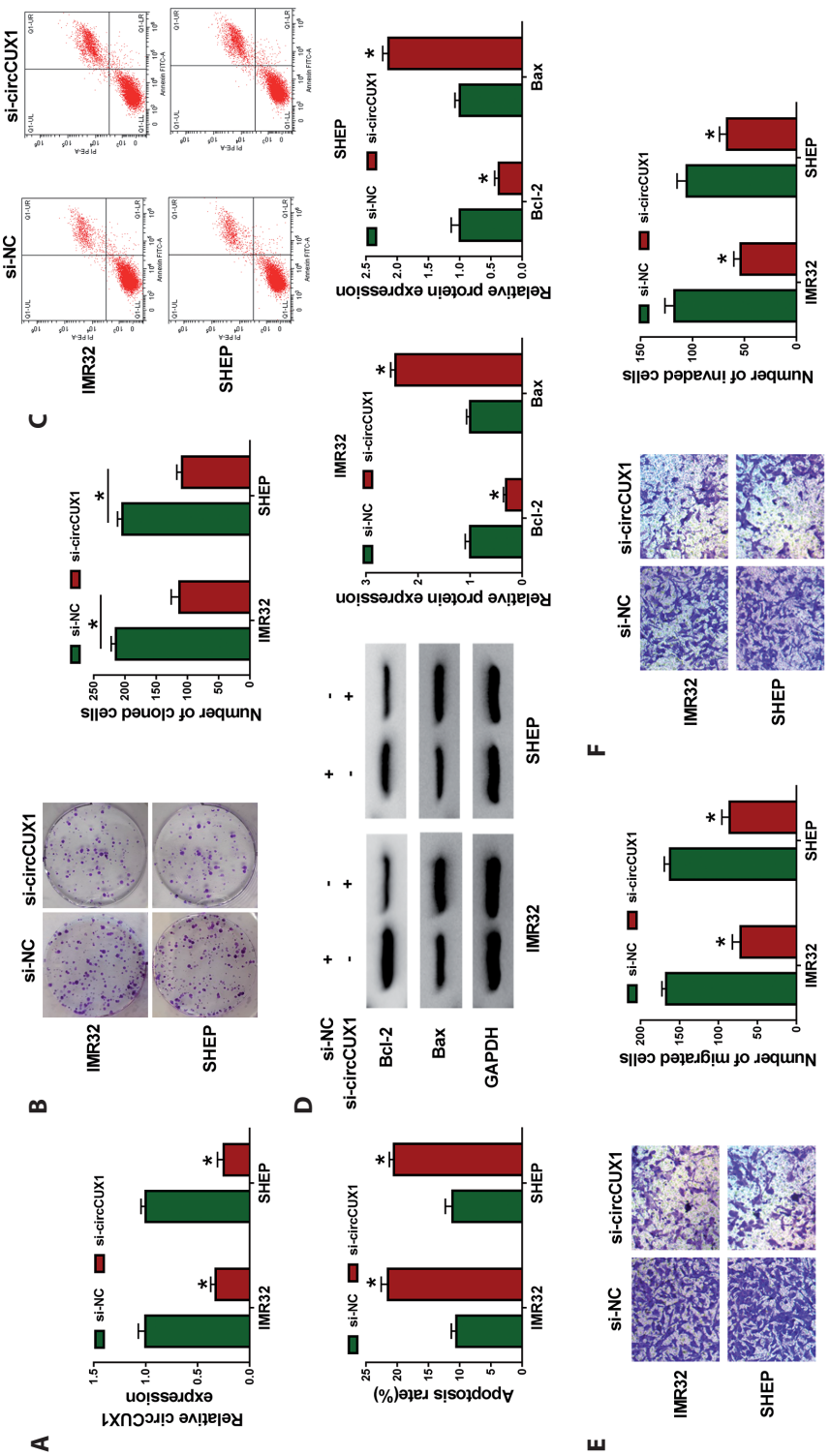

Figure 2. CircCUX1 knockdown suppresses the progression and glycolysis of neuroblastoma cells. IMR32 and SHEP cells were transfected with si-NC or si-circCUX1. **A.** circCUX1 expression was measured by qRT-PCR. **B.** Cell proliferative ability was assessed by colony formation assay. **C.** Cell apoptosis was detected by flow cytometry. **D.** The protein levels of Bcl-2 and Bax were examined using Western blot analysis. **E, F.** Cell migration and invasion were evaluated by transwell assay. **G, H.** ECAR was detected using a Seahorse XF^e 96 Extracellular Flux Analyzer. * $p < 0.05$.

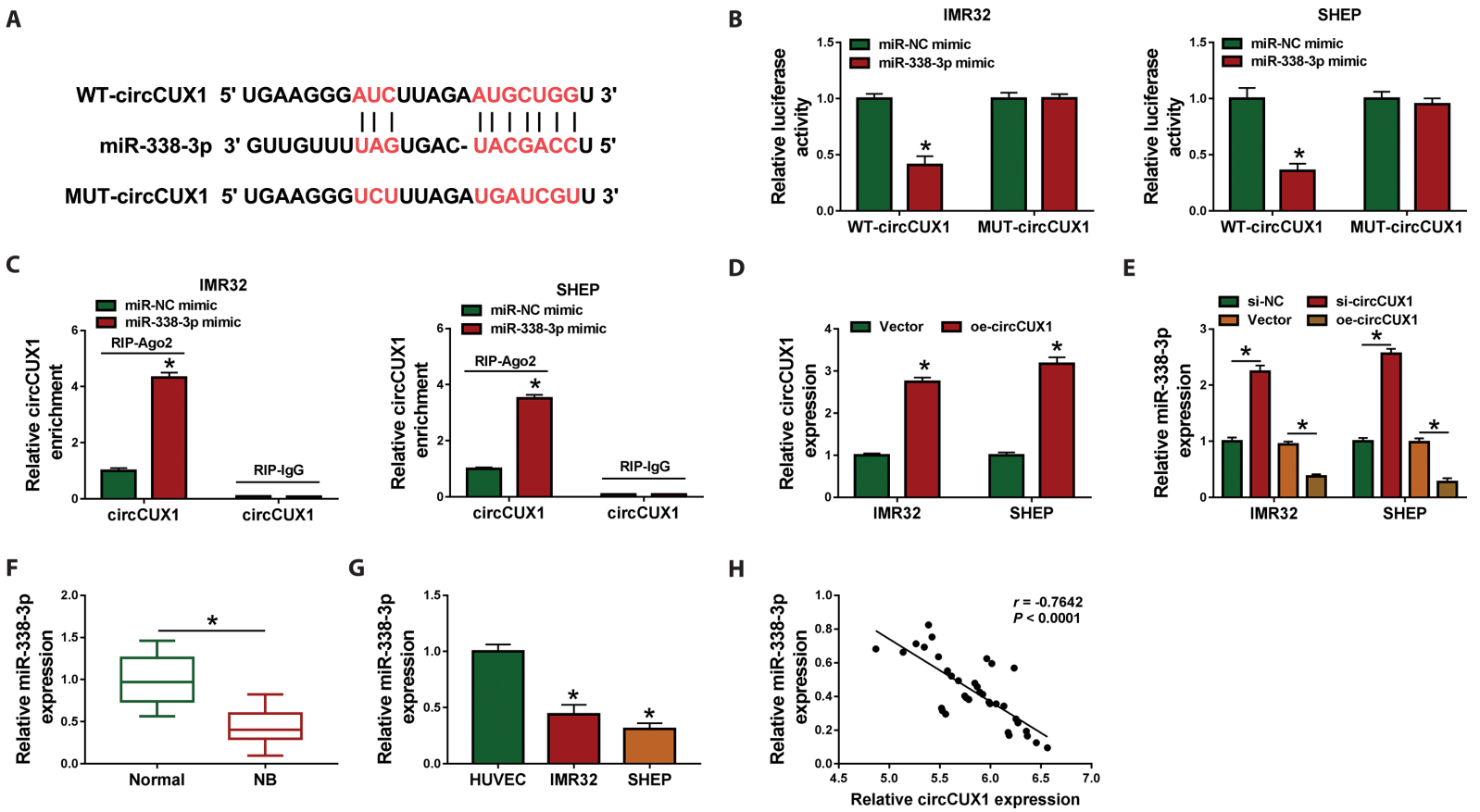

Figure 3. CircCUX1 directly interacts with miR-338-3p. **A.** The putative binding sites for circCUX1 and miR-338-3p were predicted by Circular RNA Interactome. **B.** The luciferase activity was detected in IMR32 and SHEP cells co-transfected with WT-circCUX1 or MUT-circCUX1 and miR-338-3p mimic or miR-NC mimic. **C.** RIP analysis was performed to verify whether circCUX1 bound to miR-338-3p. **D.** The level of circCUX1 was measured in IMR32 and SHEP cells transfected with Vector or oe-circCUX1. **E.** IMR32 and SHEP cells were introduced with si-NC, si-circCUX1, Vector or oe-circCUX1, miR-338-3p level was detected using qRT-PCR. **F.** The expression of miR-338-3p was examined in NB tissues ($n = 35$) and normal tissues ($n = 35$) by qRT-PCR. **G.** The level of miR-338-3p in HUVEC, IMR32 and SHEP cells was detected by qRT-PCR. **H.** Spearman's correlation analysis was used to analyze the correlation between circCUX1 and miR-338-3p in NB tissues ($n = 35$). * $p < 0.05$. NB, neuroblastoma.

of si-circCUX1 and miR-338-3p reversed these effects (Fig. 4B,C). As shown in Figure 4D, inhibition of miR-338-3p increased Bcl-2 expression and reduced Bax expression, and miR-338-3p knockdown reversed the effect of circCUX1 silencing on apoptosis-related proteins. Additionally, suppression of miR-338-3p promoted NB cell migration and invasion and alleviated the impact of circCUX1 knockdown on cell migration and invasion (Fig. 4E,F). Moreover, miR-338-3p down-regulation promoted glycolysis by increasing ECAR, and the inhibitory effect of circCUX1 silencing on glycolysis was reversed after transfection with miR-338-3p inhibitor (Fig. 4G,H). These data indicated that circCUX1 expedited NB progression and glycolysis by sponging miR-338-3p.

PHF20 is a target of miR-338-3p

To further explore the molecular mechanism of NB development, TargetScan database predicted that PHF20 might be a target for miR-338-3p (Fig. 5A). Dual-luciferase reporter assay showed that mature miR-338-3p overtly reduced the luciferase activity of WT-PHF20 reporter (Fig. 5B). We also performed RIP assay to confirm this, and the results exhibited that PHF20 was remarkably enriched in NB cells introduced with miR-338-3p mimic (Fig. 5C). In addition, the overexpression efficiency of miR-338-3p was verified by qRT-PCR (Fig. 5D). Moreover, knockdown of miR-338-3p elevated PHF20 level, and overexpression of miR-338-3p decreased PHF20 level (Fig. 5E,F). Compared with the control group, the mRNA and protein levels of PHF20 were significantly increased in NB tissues and cells (Fig. 5G–J). Furthermore, miR-338-3p expression was negatively correlated with PHF20 expression in NB tissues (Fig. 5K). Altogether, these data evidenced that miR-338-3p directly targeted PHF20.

PHF20 silencing reverses the effect of miR-338-3p inhibition on NB cells

Firstly, qRT-PCR was utilized to determine transfection efficiency of PHF20, and the results illustrated that PHF20 mRNA and protein levels in the si-PHF20 group were significantly lower than that in the si-NC group (Fig. 6A,B). To investigate whether miR-338-3p affected NB progression by regulating PHF20, we conducted a series of rescue experiments. As exhibited in Figure 6C–F, silencing of PHF20 inhibited cell proliferation, migration and invasion and induced cell apoptosis, while introduction of si-PHF20 reversed the impacts of miR-338-3p knockdown on NB progression. In addition, the ECAR was markedly decreased in the si-PHF20 group relative to the si-NC group, and the effect of miR-338-3p inhibitor on glycolysis was abrogated after transfection with si-PHF20 (Fig. 6G). These data indicated that inhibition of miR-338-3p accelerated NB progression and glycolysis *via* regulating PHF20.

CircCUX1 regulates PHF20 expression by sponging miR-338-3p

To clarify the mechanism of circCUX1 in PHF20 expression, IMR32 and SHEP cells were transfected with si-NC, si-circCUX1, si-circCUX1+miR-NC inhibitor or si-circCUX1+miR-338-3p inhibitor. As exhibited in Figure 7A, circCUX1 level was positively correlated with PHF20 level in NB tissues. The results showed that circCUX1 knockdown markedly reduced PHF20 mRNA and protein levels, while the changes were abolished by down-regulating miR-338-3p (Fig. 7B,C). These data evidenced that circCUX1 sponged miR-338-3p to regulate PHF20 expression.

CircCUX1 silencing blocks tumor growth in vivo

Moreover, we constructed a xenograft model to analyze the function of circCUX1 in tumorigenesis *in vivo*. The results revealed that tumor volume and weight in the sh-circCUX1 group were significantly decreased compared with the sh-NC group (Fig. 8A,B). Additionally, transfection with sh-circCUX1 led to a marked reduction in circCUX1 and PHF20 levels and a significant elevation in miR-338-3p level (Fig. 8C–F). Collectively, these data demonstrated that knockdown of circCUX1 hindered tumor growth *in vivo*.

Discussion

Warburg effect provides a driving force for cancer cell growth and metastasis (Icard et al. 2018). ECAR and oxygen consumption rate (OCR) are frequently-used indicators for detecting glycolysis. Besides, non-coding RNAs exert a vital regulatory effect on glucose metabolism *via* modulating glycolytic enzymes and various signaling pathways (Shankaraiah et al. 2018). However, the molecular mechanism of aerobic glycolysis in NB remains unknown.

Increasing evidence has demonstrated that circRNAs regulate biological functions by participating in competing endogenous RNA (ceRNA) mechanisms (Zhong et al. 2018). For example, Cao et al. (2020) unveiled that circRNF20 facilitated tumor progress and aerobic glycolysis in breast cancer by targeting miR-487a and mediating HIF-1α/HK2 pathway. Ding et al. (2020) suggested that circ-PRMT5 accelerated hepatoma growth and Warburg effect by serving as a ceRNA for miR-188-5p and up-regulating HK2. In addition, Chen et al. (2019) found that circRNA_100290 promoted cell progression and glycolysis in oral squamous cell carcinoma through miR-378a/GLUT1 pathway. Furthermore, extensive

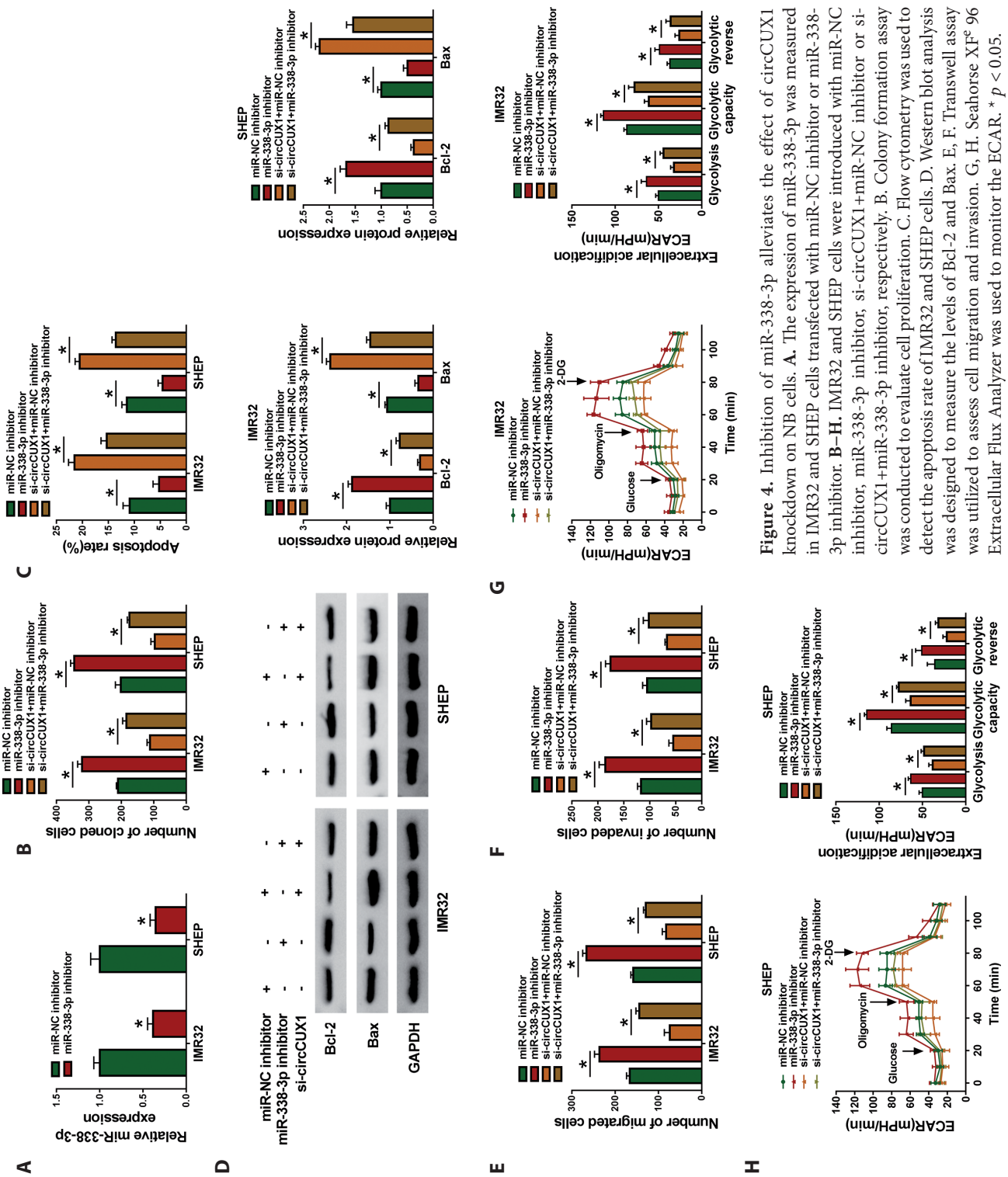

Figure 4. Inhibition of miR-338-3p alleviates the effect of circCUX1 knockdown on NB cells. **A.** The expression of miR-338-3p was measured in IMR32 and SHEP cells transfected with miR-NC inhibitor or miR-338-3p inhibitor. **B–H.** IMR32 and SHEP cells were introduced with miR-NC inhibitor, miR-338-3p inhibitor, si-circCUX1+miR-NC inhibitor or si-circCUX1+miR-338-3p inhibitor, respectively. B. Colony formation assay was conducted to evaluate cell proliferation. C. Flow cytometry was used to detect the apoptosis rate of IMR32 and SHEP cells. D. Western blot analysis was designed to measure the levels of Bcl-2 and Bax. E, F. Transwell assay was utilized to assess cell migration and invasion. G, H. Seahorse XF^e 96 Extracellular Flux Analyzer was used to monitor the ECAR. * $p < 0.05$.

research confirmed that CUX1 was strongly related to tumorigenesis and development *via* serving as a transcription factor (Ramdzan and Nepveu 2014; Wong et al. 2014). Li and Yang (2019) discovered that CUX1 and CUX1-formed circRNA (circCUX1) accelerated tumor progression and glycolysis in NB. In the current study, circCUX1 was conspicuously up-regulated in NB tissues and cells. Further, circCUX1 depletion hindered NB progression and glycolysis.

Moreover, we used bioinformatics software to predict possible targets for circCUX1 and selected miR-338-3p as a candidate. Previous studies have corroborated that miR-338-3p has antitumor effects in a variety of tumors. In thyroid cancer, miR-338-3p blocked tumor progression by inhibiting AKT3 (Sui et al. 2017). In liver cancer, miR-338-3p directly targeted SphK2 to inhibit cell proliferation (Xiao et al. 2018). In osteosarcoma, miR-338-3p suppressed cell growth and metastasis *via* down-regulating AHSA1 (Cao et al. 2018). Furthermore, miR-338-3p impeded NB progression by binding to PREX2a (Chen et al. 2013). Our research revealed that miR-338-3p level was remarkably declined in NB. More

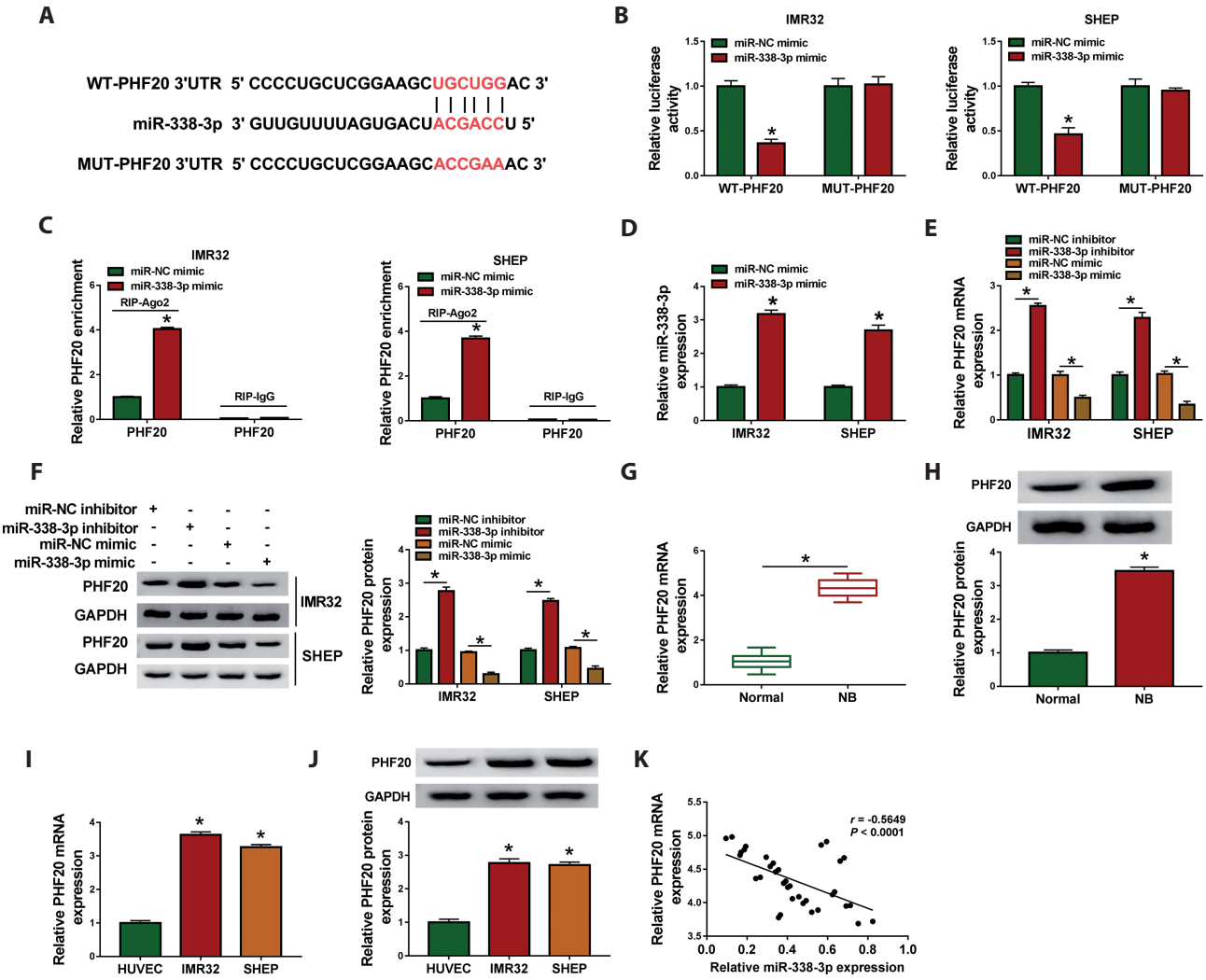

Figure 5. PHF20 is a target of miR-338-3p. **A.** The putative binding sites for miR-338-3p and PHF20 3'UTR were predicted by TargetScan. **B, C.** The relationship between miR-338-3p and PHF20 was confirmed by dual-luciferase reporter assay and RIP assay. **D.** miR-338-3p expression was measured in IMR32 and SHEP cells transfected with miR-NC mimic or miR-338-3p mimic. **E, F.** IMR32 and SHEP cells were introduced with miR-NC inhibitor, miR-338-3p inhibitor, miR-NC mimic or miR-338-3p mimic, and the expression of PHF20 was examined by qRT-PCR and Western blot. **G, H.** The mRNA and protein levels of PHF20 were measured in NB tissues (n = 35) and normal tissues (n = 35). **I, J.** The mRNA and protein levels of PHF20 were detected in HUVEC, IMR32 and SHEP cells. **K.** The correlation between miR-338-3p and PHF20 in NB tissues (n = 35) was analyzed by Spearman's correlation analysis. * $p < 0.05$. NB, neuroblastoma.

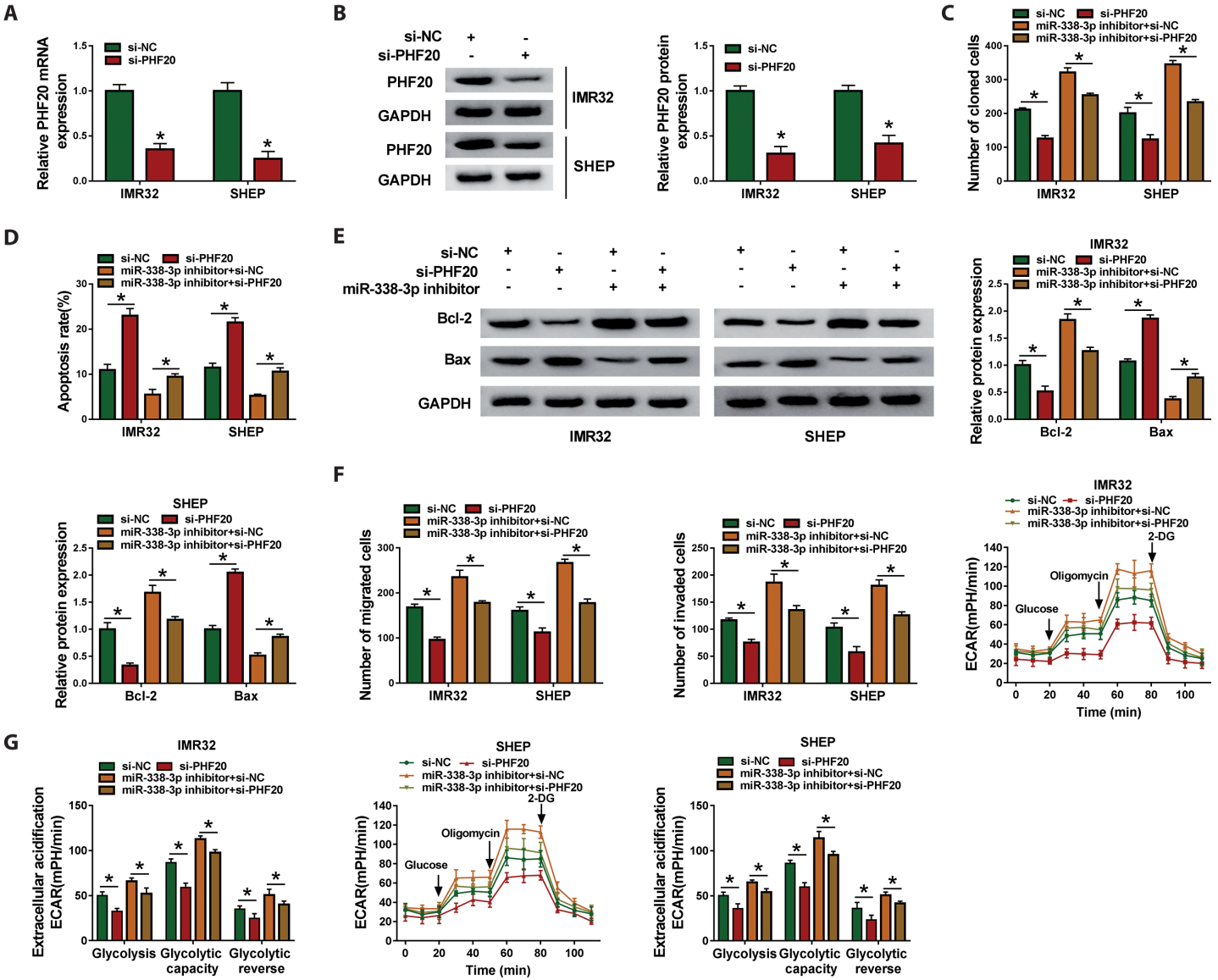

Figure 6. PHF20 silencing reverses the effect of miR-338-3p inhibition on neuroblastoma cells. **A, B.** The mRNA and protein levels of PHF20 were detected in IMR32 and SHEP cells transfected with si-NC or si-PHF20. **C–G.** IMR32 and SHEP cells were introduced with si-NC, si-PHF20, miR-338-3p inhibitor+si-NC or miR-338-3p inhibitor+si-PHF20, respectively. C. Cell proliferation was evaluated by colony formation assay. D. Cell apoptosis was monitored by flow cytometry. E. The protein levels of Bcl-2 and Bax were examined using Western blot. F. Cell migration and invasion were detected by transwell assay. G. ECAR was assessed using a Seahorse XF^e 96 Extracellular Flux Analyzer. * $p < 0.05$.

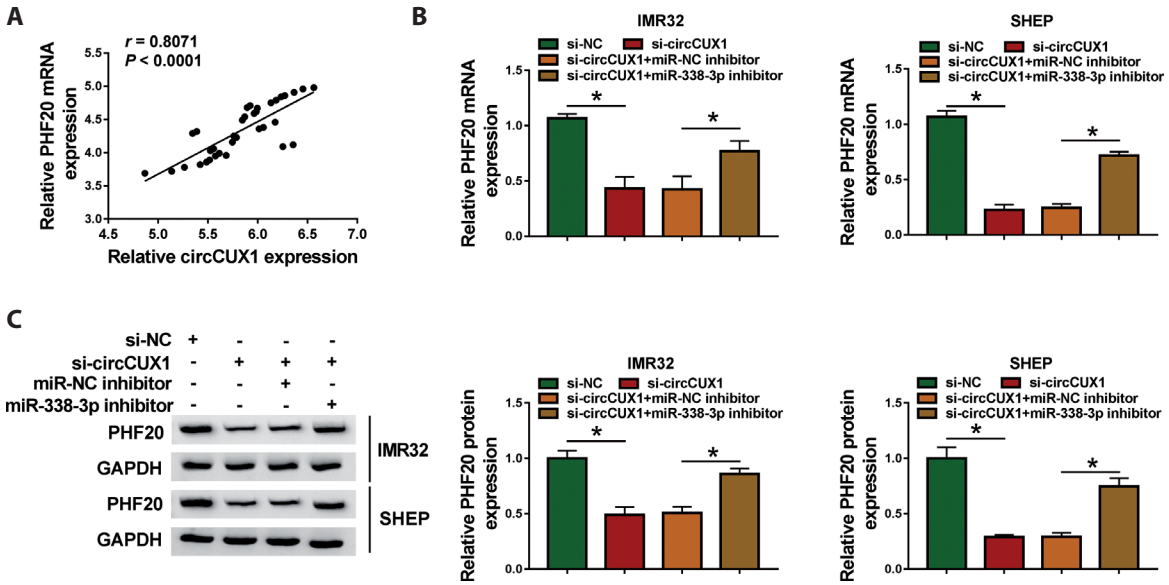

Figure 7. circCUX1 regulates PHF20 expression by sponging miR-338-3p. **A.** Spearman's correlation analysis was performed to analyze the correlation between circCUX1 and PHF20 in neuroblastoma tissues (n = 35). **B, C.** IMR32 and SHEP cells were introduced with si-NC, si-circCUX1, si-circCUX1+miR-NC inhibitor or si-circCUX1+miR-338-3p inhibitor, and the mRNA and protein levels of PHF20 were measured by qRT-PCR and Western blot. * $p < 0.05$.

importantly, miR-338-3p down-regulation attenuated the inhibition of circCUX1 depletion on NB progression and Warburg effect.

Compelling evidence has demonstrated miRNAs negatively regulate gene expression by base-pairing to mRNA 3'UTR (Fabian et al. 2010). In this research, we first validated

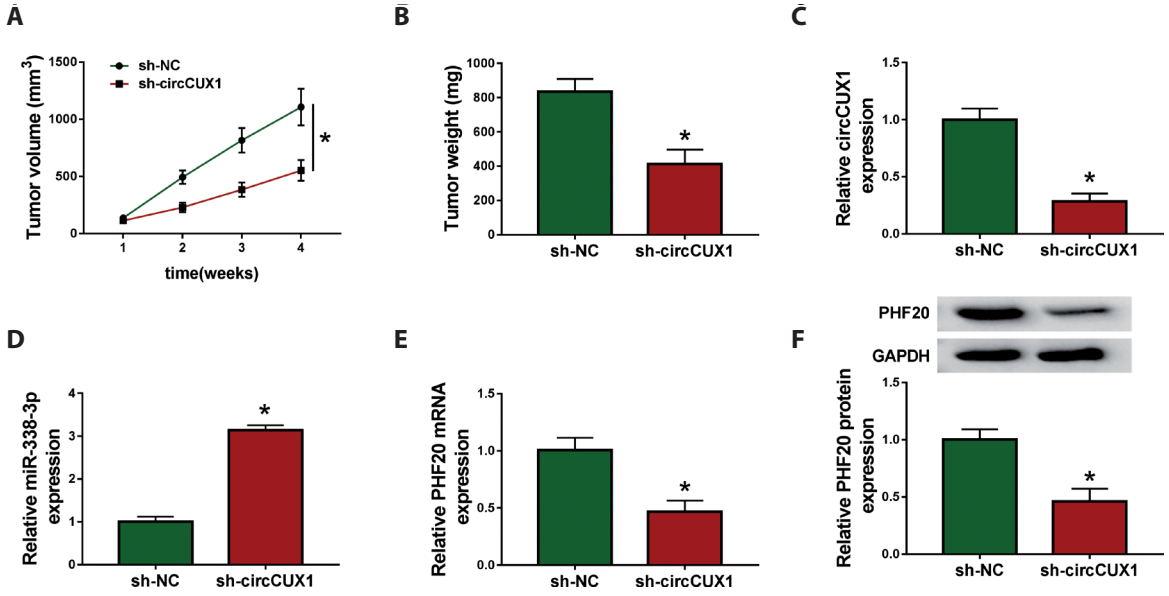

Figure 8. circCUX1 silencing blocks tumor growth *in vivo*. SHEP cells transfected with sh-NC or sh-circCUX1 were subcutaneously injected into the nude mice. **A.** Tumor volume was measured once a week. **B.** After four weeks, the mice were killed and the tumors were weighed. **C, D.** The levels of circCUX1 and miR-338-3p were examined by qRT-PCR. **E, F.** The mRNA and protein levels of PHF20 were detected by qRT-PCR and Western blot. * $p < 0.05$.

that miR-338-3p targeted PHF20 and negatively modulated PHF20. In glioblastoma, PHF20 participated in tumor occurrence and development by mediating a series of tumor-related genes and activating apoptosis-related signaling pathways (Liu et al. 2017). Long and Zhao (2018) presented that PHF20 contributed to maintaining NB cell stemness and elevating aggressiveness via activating SOX2 and OCT4. Consistent with our research, PHF20 expression was overtly up-regulated in NB. Furtherly, knockdown of PHF20 overturned the promotion of miR-338-3p down-regulation on NB progression and glycolysis.

In conclusion, our findings unveiled that circCUX1 triggered the progression and glycolysis of NB by serving as a ceRNA for miR-338-3p and up-regulating PHF20. These results hinted that circCUX1 might be a novel therapeutic marker for NB.

Conflict of interest. The authors declare that they have no financial conflicts of interest.

Ethics approval and consent to participate. The design of this protocol follows the tenets of the Declaration of Helsinki, approved by the Ethics Committee of The First People's Hospital of Lianyungang.

Funding. This study was supported by Jiangsu Provincial Health and Family Planning Commission (Grant No. F201553).

References

Brodeur GM, Bagatell R (2014): Mechanisms of neuroblastoma regression. Nat. Rev. Clin. Oncol. **11,** 704-713 https://doi.org/10.1038/nrclinonc.2014.168

Cao L, Wang M, Dong Y, Xu B, Chen J, Ding Y, Qiu S, Li L, Karamfilova Zaharieva E, Zhou X et al. (2020): Circular RNA circRNF20 promotes breast cancer tumorigenesis and Warburg effect through miR-487a/HIF-1alpha/HK2. Cell Death Dis. **11,** 145 https://doi.org/10.1038/s41419-020-2336-0

Cao R, Shao J, Hu Y, Wang L, Li Z, Sun G, Gao X (2018): microRNA-338-3p inhibits proliferation, migration, invasion, and EMT in osteosarcoma cells by targeting activator of 90 kDa heat shock protein ATPase homolog 1. Cancer Cell. Int. **18,** 49 https://doi.org/10.1186/s12935-018-0551-x

Chen X, Pan M, Han L, Lu H, Hao X, Dong Q (2013): miR-338-3p suppresses neuroblastoma proliferation, invasion and migration through targeting PREX2a. FEBS Lett. **587,** 3729-3737 https://doi.org/10.1016/j.febslet.2013.09.044

Chen X, Yu J, Tian H, Shan Z, Liu W, Pan Z, Ren J (2019): Circle RNA hsa_circRNA_100290 serves as a ceRNA for miR-378a to regulate oral squamous cell carcinoma cells growth via Glucose transporter-1 (GLUT1) and glycolysis. J. Cell Physiol. **234,** 19130-19140 https://doi.org/10.1002/jcp.28692

Cui X, Wang J, Guo Z, Li M, Li M, Liu S, Liu H, Li W, Yin X, Tao J et al (2018): Emerging function and potential diagnostic value of circular RNAs in cancer. Mol. Cancer **17,** 123 https://doi.org/10.1186/s12943-018-0877-y

Ding Z, Guo L, Deng Z, Li P (2020): Circ-PRMT5 enhances the proliferation, migration and glycolysis of hepatoma cells by targeting miR-188-5p/HK2 axis. Ann. Hepatol. **19,** 269-279 https://doi.org/10.1016/j.aohep.2020.01.002

Fabian MR, Sonenberg N, Filipowicz W (2010): Regulation of mRNA translation and stability by microRNAs. Annu. Rev. Biochem. **79,** 351-379 https://doi.org/10.1146/annurev-biochem-060308-103103

Farazi TA, Spitzer JI, Morozov P, Tuschl T (2011): miRNAs in human cancer. J. Pathol. **223,** 102-115 https://doi.org/10.1002/path.2806

He XY, Tan ZL, Mou Q, Liu FJ, Liu S, Yu CW, Zhu J, Lv LY, Zhang J, Wang S et al. (2017): microRNA-221 enhances MYCN via targeting nemo-like kinase and functions as an oncogene related to poor prognosis in neuroblastoma. Clin. Cancer Res. **23,** 2905-2918 https://doi.org/10.1158/1078-0432.CCR-16-1591

Icard P, Shulman S, Farhat D, Steyaert JM, Alifano M, Lincet H (2018): How the Warburg effect supports aggressiveness and drug resistance of cancer cells? Drug Resist. Updat. **38,** 1-11 https://doi.org/10.1016/j.drup.2018.03.001

Kristensen LS, Andersen MS, Stagsted LVW, Ebbesen KK, Hansen TB, Kjems J (2019): The biogenesis, biology and characterization of circular RNAs. Nat. Rev. Genet. **20,** 675-691 https://doi.org/10.1038/s41576-019-0158-7

Li H, Yang F, Hu A, Wang X, Fang E, Chen Y, Li D, Song H, Wang J, Guo Y et al (2019): Therapeutic targeting of circ-CUX1/EWSR1/MAZ axis inhibits glycolysis and neuroblastoma progression. EMBO Mol. Med. **11,** e10835 https://doi.org/10.15252/emmm.201910835

Li Y, Park J, Piao L, Kong G, Kim Y, Park KA, Zhang T, Hong J, Hur GM, Seok JH et al. (2013): PKB-mediated PHF20 phosphorylation on Ser291 is required for p53 function in DNA damage. Cell Signal. **25,** 74-84 https://doi.org/10.1016/j.cellsig.2012.09.009

Liu T, Zhang T, Zhou F, Wang J, Zhai X, Mu N, Park J, Liu M, Liu W, Shang P et al. (2017): Identification of genes and pathways potentially related to PHF20 by gene expression profile analysis of glioblastoma U87 cell line. Cancer Cell. Int. **17,** 87 https://doi.org/10.1186/s12935-017-0459-x

Liu X, Peng H, Liao W, Luo A, Cai M, He J, Zhang X, Luo Z, Jiang H, Xu L (2018): MiR-181a/b induce the growth, invasion, and metastasis of neuroblastoma cells through targeting ABI1. Mol. Carcinog. **57,** 1237-1250 https://doi.org/10.1002/mc.22839

Long W, Zhao W, Ning B, Huang J, Chu J, Li L, Ma Q, Xing C, Wang HY, Liu Q et al. (2018): PHF20 collaborates with PARP1 to promote stemness and aggressiveness of neuroblastoma cells through activation of SOX2 and OCT4. J. Mol. Cell. Biol. **10,** 147-160 https://doi.org/10.1093/jmcb/mjy007

Louis CU, Shohet JM (2015): Neuroblastoma: molecular pathogenesis and therapy. Annu. Rev. Med. **66,** 49-63 https://doi.org/10.1146/annurev-med-011514-023121

Mao F, Zhang J, Cheng X, Xu Q (2019): miR-149 inhibits cell proliferation and enhances chemosensitivity by targeting CDC42 and BCL2 in neuroblastoma. Cancer Cell Int. **19,** 357

https://doi.org/10.1186/s12935-019-1082-9
Maris JM, Hogarty MD, Bagatell R, Cohn SL (2007): Neuroblastoma. Lancet **369,** 2106-2120 https://doi.org/10.1016/S0140-6736(07)60983-0
Matthay KK (1995): Neuroblastoma: a clinical challenge and biologic puzzle. CA Cancer J. Clin. **45,** 179-192 https://doi.org/10.3322/canjclin.45.3.179
Park S, Kim D, Dan HC, Chen H, Testa JR, Cheng JQ (2012): Identification of Akt interaction protein PHF20/TZP that transcriptionally regulates p53. J. Biol. Chem. **287,** 11151-11163 https://doi.org/10.1074/jbc.M111.333922
Ramdzan ZM, Nepveu A (2014): CUX1, a haploinsufficient tumour suppressor gene overexpressed in advanced cancers. Nat. Rev. Cancer **14,** 673-682 https://doi.org/10.1038/nrc3805
Shankaraiah RC, Veronese A, Sabbioni S, Negrini M (2018): Non-coding RNAs in the reprogramming of glucose metabolism in cancer. Cancer Lett. **419,** 167-174 https://doi.org/10.1016/j.canlet.2018.01.048
Sui GQ, Fei D, Guo F, Zhen X, Luo Q, Yin S, Wang H (2017): MicroRNA-338-3p inhibits thyroid cancer progression through targeting AKT3. Am. J. Cancer Res. **7,** 1177-1187
Vander Heiden MG, Cantley LC, Thompson CB (2009): Understanding the Warburg effect: the metabolic requirements of cell proliferation. Science **324,** 1029-1033 https://doi.org/10.1126/science.1160809
Wong CC, Martincorena I, Rust AG, Rashid M, Alifrangis C, Alexandrov LB, Tiffen JC, Kober C, Green AR, Massie CE et al. (2014): Inactivating CUX1 mutations promote tumorigenesis. Nat. Genet. **46,** 33-38 https://doi.org/10.1038/ng.2846
Xiao G, Wang Q, Li B, Wu X, Liao H, Ren Y, Ai N (2018): MicroRNA-338-3p suppresses proliferation of human liver cancer cells by targeting SphK2. Oncol. Res. **26,** 1183-1189 https://doi.org/10.3727/096504018X15151495109394
Ye M, Hou H, Shen M, Dong S, Zhang T (2020): Circular RNA circFOXM1 Plays a Role in Papillary Thyroid Carcinoma by Sponging miR-1179 and Regulating HMGB1 Expression. Mol. Ther. Nucleic Acids **19,** 741-750 https://doi.org/10.1016/j.omtn.2019.12.014
Zhong Y, Du Y, Yang X, Mo Y, Fan C, Xiong F, Ren D, Ye X, Li C, Wang Y et al (2018): Circular RNAs function as ceRNAs to regulate and control human cancer progression. Mol. Cancer **17,** 79 https://doi.org/10.1186/s12943-018-0827-8
Zhou J, Zhang S, Chen Z, He Z, Xu Y, Li Z (2019): CircRNA-ENO1 promoted glycolysis and tumor progression in lung adenocarcinoma through upregulating its host gene ENO1. Cell Death Dis. **10,** 885 https://doi.org/10.1038/s41419-019-2127-7

Received: September 2, 2020
Final version accepted: December 1, 2020